Surface Review and Letters, Vol. 10, No. 6 (2003) 963–980

World Scientific
www.worldscientific.com

ELECTRICAL CONDUCTION THROUGH SURFACE SUPERSTRUCTURES MEASURED BY MICROSCOPIC FOUR-POINT PROBES

SHUJI HASEGAWA, ICHIRO SHIRAKI, FUHITO TANABE, REI HOBARA,
TAIZO KANAGAWA, TAKEHIRO TANIKAWA and IWAO MATSUDA
Department of Physics, University of Tokyo,
7-3-1 Hongo, Bunkyo-ku, Tokyo 113-0033, Japan

CHRISTIAN L. PETERSEN
Capres A/S, DTU Bldg. 404 east, DK-2800, Lyngby, Denmark

TORBEN M. HANSEN, PETER BOGGILD and FRANCOIS GREY
Microelectronics Center, Denmark Technical University,
Bldg. 345 east, DK-2800, Lyngby, Denmark

Received 21 May 2003

For *in-situ* measurements of the local electrical conductivity of well-defined crystal surfaces in ultra-high vacuum, we have developed two kinds of microscopic four-point probe methods. One involves a "four-tip STM prober," in which four independently driven tips of a scanning tunneling microscope (STM) are used for measurements of four-point probe conductivity. The probe spacing can be changed from 500 nm to 1 mm. The other method involves monolithic micro-four-point probes, fabricated on silicon chips, whose probe spacing is fixed around several μm. These probes are installed in scanning-electron-microscopy/electron-diffraction chambers, in which the structures of sample surfaces and probe positions are observed *in situ*. The probes can be positioned precisely on aimed areas on the sample with the aid of piezoactuators. By the use of these machines, the surface sensitivity in conductivity measurements has been greatly enhanced compared with the macroscopic four-point probe method. Then the conduction through the topmost atomic layers (surface-state conductivity) and the influence of atomic steps on conductivity can be directly measured.

Keywords: Four-point probe conductivity measurement; surface-state conductivity; scanning tunneling microscopy; scanning electron microscopy.

1. Introduction

The topmost layers of crystal surfaces are known to have characteristic electronic band structures that are sometimes quite different from those in the inner bulk. While such *surface states* have so far been well studied, for example by photoemission spectroscopy and scanning tunneling spectroscopy, the electrical conduction through them, *surface-state conductance* has been little studied because of its difficulty.[1,2] Due to the thinness of the surface atomic layers, the surface-state conductance is usually much lower than the conductance through the underlying bulk crystal. Furthermore, surface defects like steps and domain boundaries greatly perturb the electron conduction through the surface states. These facts have prevented the direct detection and quantitative measurement of the intrinsic surface-state conductivity. Since, however, the surface-state conductance, *electron conduction through only one or two atomic layers*, is an essential issue in the study of electronic transport in nanometer-scale regions or objects, it has recently attracted much interest, and large amounts of efforts are now made to detect and measure it. Here we introduce a novel tool,

microscopic four-point probes, and demonstrate their effectiveness for such purposes.[3–7]

Before going into the details, we should describe previous trials with macroscopic four-probe methods in measuring the electrical conductance of atomic layers of crystal surfaces and/or monolayer-range thin films. The conductance of metal atomic layers on insulating substrates was frequently measured in relation to the growth style and morphology of atomic layers.[8–13] Those studies have revealed intriguing phenomena, such as classical/quantum size effects, insulator-to-metal transition, oscillatory changes in the sign of Hall coefficients and in the critical temperature of the superconductivity of the metal films as a function of the film thickness and atomic structures. These films are basically assumed to be just "thinned bulk crystals," having the same electronic band structures as the bulk crystals.

The conductance of surface-state bands of bulk crystals, on the other hand, was measured in several different ways. One was by observing a conductance increase due to carrier doping into a surface-state band by adsorbates on the surface, which was revealed by combing the conductance measurements with photoemission spectroscopy for the band-structure measurements.[1,2,14] The observed conductance change was separated from the bulk conductance by taking into account the change in surface-state bands. Another way to extract the surface-state conductance was to use a so-called SOI (semiconductor-on-insulator) crystal where the substrate conductance was effectively negligible due to its thinness.[15] This was successfully employed in detecting a conductance change due to a phase transition of the surface structure. Those results, achieved by using macroscopic four-point probes with 1–10 mm probe spacing, needed some efforts to eliminate the conductance of substrate bulks.

A unique technique, so-called scanning potentiometry using a single-tip scanning tunneling microscope (STM), was employed to measure the surface-state conductance.[16] Due to a voltage drop by a finite resistance of the sample surface, the STM images showed characteristic contrasts, which were compared with simulation results to deduce the surface-state conductance. Another example in detecting the surface-state conductance using STM is leakage-current measurements at point contacts between the STM tip and sample surfaces.[17] Due to a Schottky barrier between the STM tip and a silicon substrate, the leak current was attributed to the current flowing along the surface-state band. In those measurements using a single-tip STM, one needed some simulation or assumption to quantify the results of conductance.

A four-probe method is the most direct and common one for measuring the electrical conductance of samples. So we first briefly introduce the principle of the four-point probe method and electrical conduction near a semiconductor surface, and then explain why a *microscopic* four-point probe is needed to detect and measure the surface-state conductance.

When, as shown in Fig. 1(a), the outer pair of probes are put in contact with a sample surface and a voltage is applied between them, a current I flows through the sample. The inner pair of probes, which are also put in contact with the sample, pick up a voltage drop V along the surface owing to the resistance of the sample. Thus one can obtain a four-point probe resistance $R = V/I$ (strictly speaking, it is multiplied by a correction factor depending on the specimen shape and probe arrangement). Owing to this configuration, one can correctly measure the resistance of a sample without any influence of contact resistance at the probe contacts, irrespective of whether the probe contacts are ohmic or Schottky-type. This is because no current virtually flows through the inner pair of contacts, so that no voltage drops occur at the probe contacts. This is a great advantage in the four-point probe method.

When the specimen is a semiconductor crystal, the measurement current will in principle flow through three channels in the sample:[18]

(1) *Surface states* on the topmost atomic layers (when a well-ordered surface superstructure is developed),
(2) Bulk states in the *surface space-charge layer* beneath the surface (when the bulk bands bend beneath the surface, the carrier concentration can be different from in the inner bulk), and
(3) Bulk states in the interior of crystal (which do not depend on the surface structures and states).

In general, the resistance measured by the four-point probe method contains the contributions from all of these channels, and it is difficult to separate them. In the case of measurements in air, however, the sample surface is usually dirty and does not have a well-ordered surface superstructure, so that the

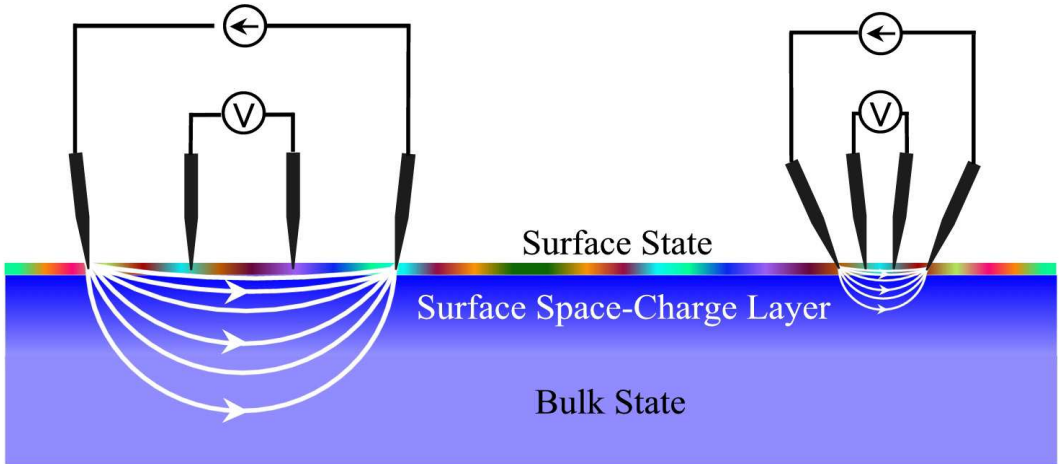

Fig. 1. (a) Macro- and (b) micro-four-point probe methods to measure electrical conductance. The distribution of current flowing through a semiconductor specimen is schematically drawn.

measured resistance is interpreted to be only the bulk value. But under special conditions where the bands bend sharply under the surface to produce a carrier accumulation layer, or in ultrahigh vacuum (UHV) where the sample crystal has a well-ordered surface superstructure with a conductive surface-state band, the contributions from the surface layers cannot be ignored. Even under such situations, however, the surface contributions have been considered to be very small, because, as shown in Fig. 1(a), the measurement current flows mainly through the underlying bulk in the case of *macroscopic* probe spacing.

If, as shown in Fig. 1(b), one makes the probe spacing as small as the thickness of the space-charge layer or less than it, the measurement current will mainly flow through the surface region, which diminishes the bulk contribution in conductance measurement. This *microscopic four-point probe* method thus has a higher surface sensitivity. However, this picture looks too naïve, because the real current distribution may be complicated due to a possible barrier between the surface state and bulk state and/or a possible *pn* junction between the surface space-charge layer and underlying bulk state. But the experimental results described below show qualitatively the validity of this intuitive picture in Fig. 1.

Microscopic four-point probes have another advantage: they enable local measurements by selecting the area of concern with the aid of microscopes, so that the influence of observable defects can be avoided or intentionally included. Furthermore, by scanning the probes laterally on the sample surface, one can obtain a map of conductivity with a high spatial resolution.[19]

Here, two kinds of microscopic four-point probes are introduced with some preliminary data.

2. Independently Driven Four-Tip STM Prober

2.1. *Apparatus*

Figure 2 shows a series of scanning electron micrographs (SEM's) of four tips during operation of the four-tip STM prober.[5,6] The tips are chemically etched W wires. While the probe spacing is as large as 1 mm in (a), the probes are brought together into about 1 μm spacing in (b)–(d). This apparatus enables independent STM operation by each tip, and also four-point probe conductivity measurements with various probe arrangements and spacing. The four tips are made to approach the sample surface simultaneously with feedback control by tunnel current detection. After that, the tips are made to move forward by a definite distance by piezo-actuators to make direct contacts with the sample surface, and then the four-point probe conductivity measurement is done. The preamplifier is swiftly switched from the tunnel-current mode to the four-point probe conductivity measurement mode.

Figure 3 is a photograph of the goniometer stage on which the sample and four sets of scanners are mounted. Each tip points to the sample at 45° from

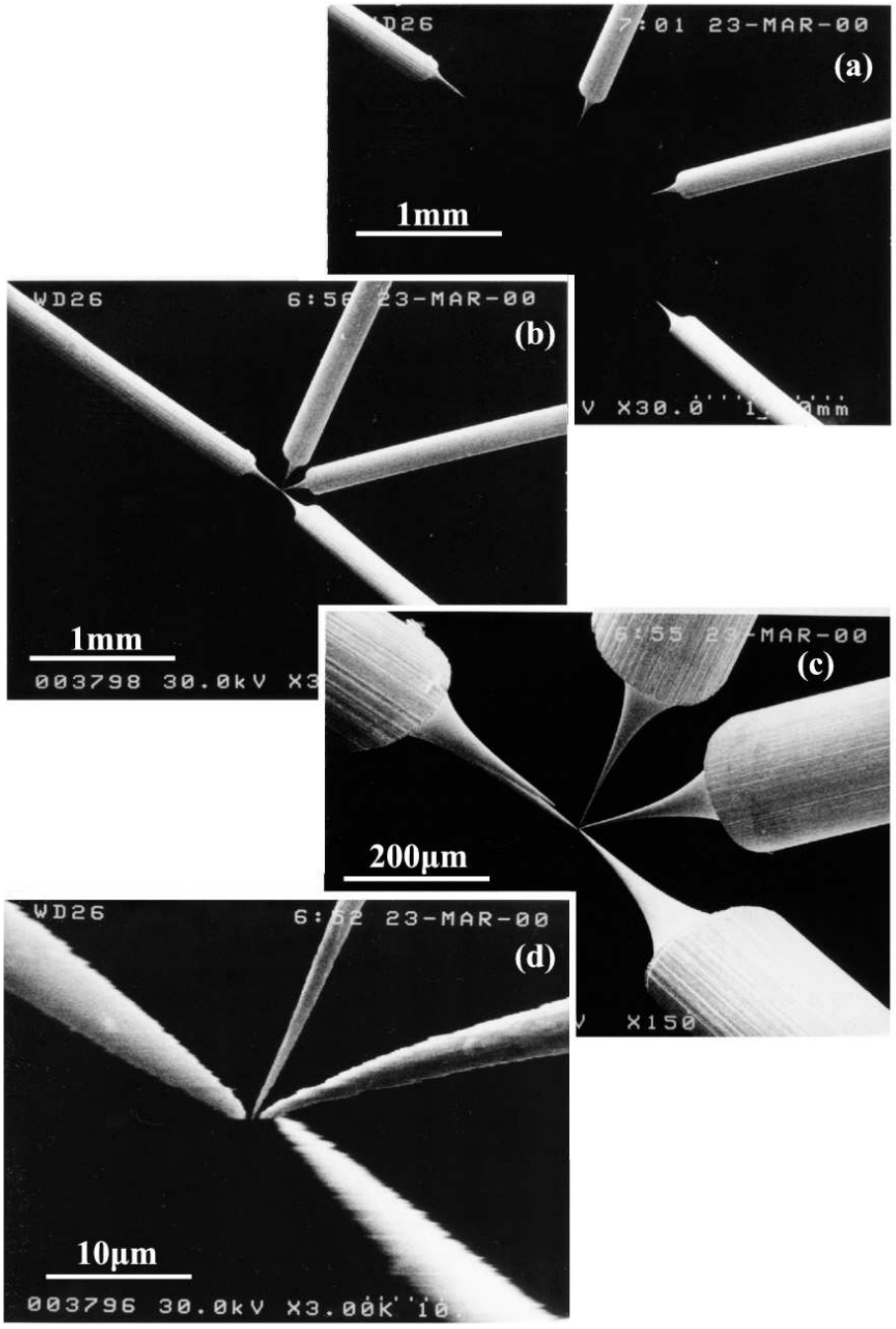

Fig. 2. SEM images of four tips of the independently driven four-tip STM prober.

the sample surface, and is driven by a special type of piezo-scanner for fine positioning and by three sets of piezo-actuators (Microslide, Omicron) for coarse motion. Figure 4 is a schematic of the apparatus in a UHV chamber. The goniometer stage enables parallel shifts in three directions and tilt rotation around an axis. The sample can be rotated azimuthally by 360° with respect to the stage. These positioning mechanisms enable fine adjustments with respect to the SEM electron beam, for making reflection high energy electron diffraction (RHEED) and scanning reflection electron microscopy (SREM) observations

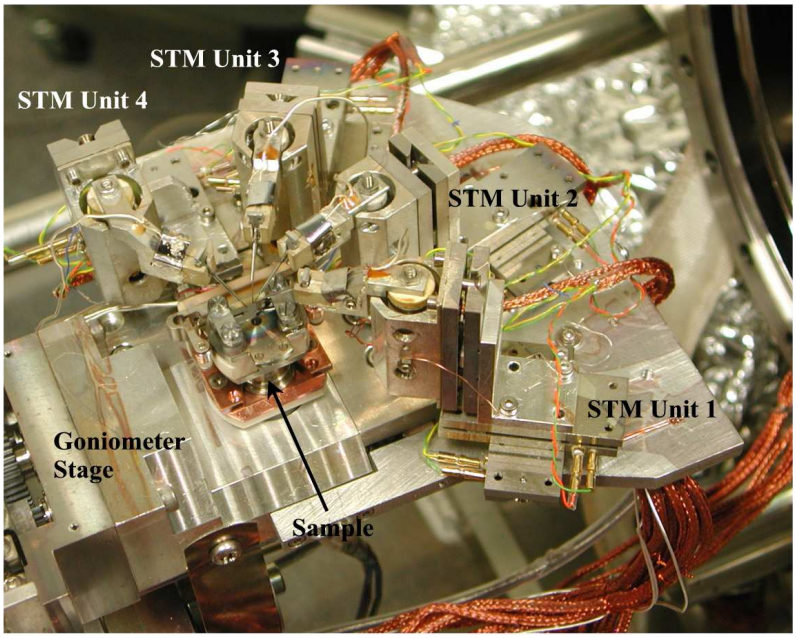

Fig. 3. Photograph of a goniometer stage of the independently driven four-tip STM prober.

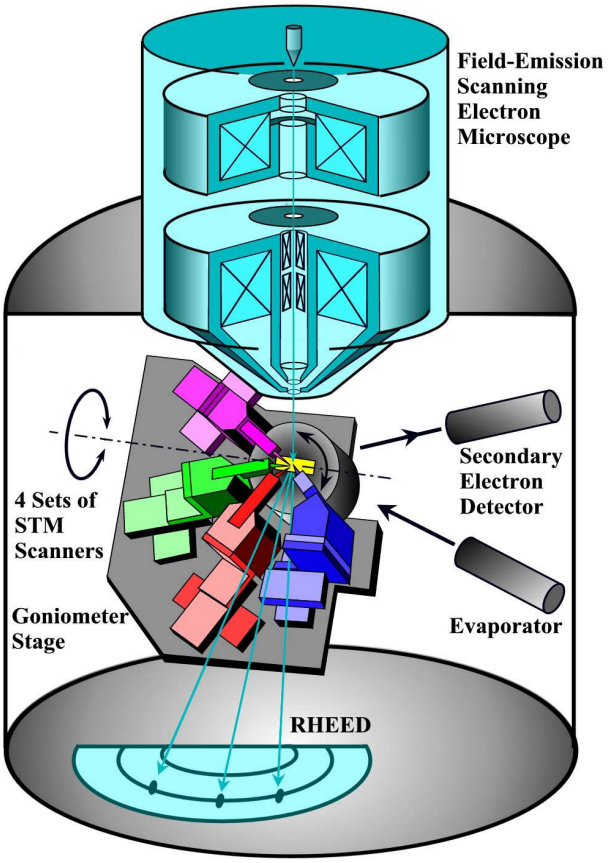

Fig. 4. A schematic of the independently driven four-tip STM prober, installed in a UHV-SEM-RHEED system.

of the sample surface simultaneously. These supplementary electron microscopy/diffraction techniques are indispensable not only for positioning the four tips properly, but also for confirming the surface structures of the sample. The tips and the sample can be exchanged and installed by transfer rods from load-lock chambers without breaking vacuum.

The STM images by each tip do not yet have atomic resolutions, but monatomic steps are resolved. The details of this apparatus are given in Ref. 5.

2.2. *Probe-spacing dependence*

We shall introduce preliminary results for two typical surface superstructures on a Si(111) crystal. One is the Si(111)–(7×7) clean surface, obtained by flash heating up to 1250°C in UHV, and the other is the Si(111)-$(\sqrt{3} \times \sqrt{3})$-Ag superstructure, obtained by depositing one atomic layer of Ag on the 7×7 surface kept at 450°C. Their atomic arrangements and surface electronic states are already well understood; the details are in e.g. Refs. 1, 2 and 20. The latter surface has a two-dimensional free-electron-like metallic surface-state band, while the former surface has a localized metallic surface state (dangling-bond state). Since the characters of their electronic structures are so different, they provide

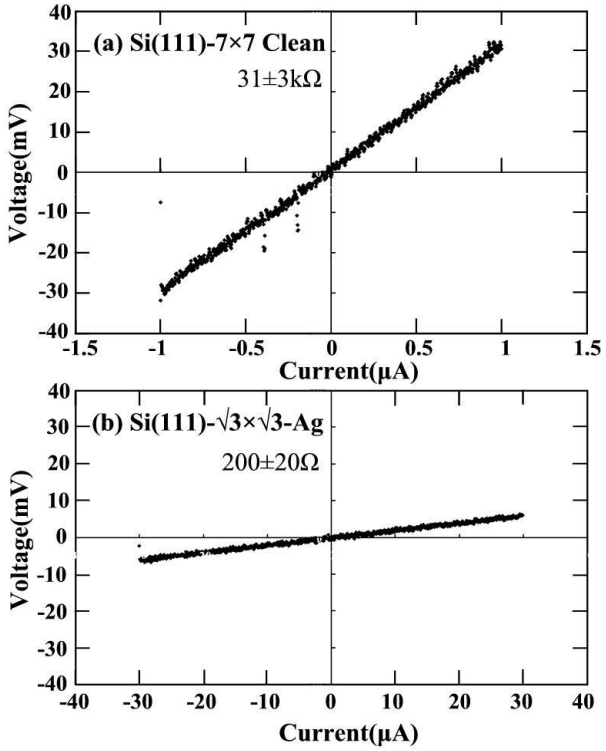

Fig. 5. I–V curves measured at room temperature with the four-tip STM prober at probe spacing of 5 μm for (a) Si(111)-(7 × 7) clean and (b) Si(111)-($\sqrt{3} \times \sqrt{3}$)-Ag surfaces, respectively. Through fitting the curve by a straight line, the differential resistance is obtained from the gradient.

comparative testing grounds for the surface conductance measurement.

Figures 5(a) and 5(b) show current–voltage characteristics for the respective surfaces measured at room temperature (RT) in UHV with a four-tip arrangement of 5 μm spacing (i.e. 15 μm between the current probes). The sample Si crystal was $3 \times 15 \times 0.4$ mm^3 in size, n-type, and 5–15 Ω cm in bulk resistivity. The voltage drop measured by the inner pair of probes (in the vertical axis) is linearly proportional to the current fed through the outer pair of probes (in the horizontal axis). From the gradients of the curves, the differential resistance is found to be 31 ± 3 kΩ for the 7×7 surface and 200 ± 20 Ω for the ($\sqrt{3} \times \sqrt{3}$)-Ag surface. The error bars mean data scattering depending on the measured areas on the same surfaces.

Only one atomic layer of Ag deposition on a Si crystal 0.4 mm thick makes the electrical resistance decrease by more than two orders of magnitude! Many readers cannot believe this result at once. But we confirmed the reproducibility with several samples, and confirmed it also with the additional data described below. When one compares this result with the previous ones by macroscopic four-point probes of about 10 mm probe spacing in which the difference in resistance between the two surfaces was only around 10%,[21] it is evident that *the miniaturization of four-point probes makes the resistance measurements very sensitive to the surface structures.* This is the expectation in Fig. 1.

In order to convince the readers of this result, we did the systematic four-point probe measurements by changing the probe spacing from 1 mm to 1 μm; the four tips can be independently driven in this machine, so that we can arrange the probes arbitrarily on the sample surface to change the probe spacing continuously. The result is shown in Fig. 6.[5,6] The horizontal axis is the probe spacing d (spacing between the two probes), and the vertical axis is the differential resistance derived from the IV curves similar to those in Fig. 5 (the values are without geometrical-factor corrections). Data points of red circles are for the 7×7 clean surface, and blue squares are for the ($\sqrt{3} \times \sqrt{3}$)-Ag surface. This clearly shows that the probe-spacing dependence of resistance is quite different between the two surfaces. For the 7×7 surface, the resistance changes significantly in a characteristic way, depending on the probe spacing; especially, it drastically increases at $d < 10$ μm. For the ($\sqrt{3} \times \sqrt{3}$)-Ag surface, on the other hand, the change in resistance with d is much more moderate; the resistance gradually decreases with decreasing d, which is opposite to the tendency for the 7×7 surface. *These differences mean that the nature of electron conduction is quite different between the two surfaces.* While the difference in resistance between the two surfaces is negligibly small at $d \sim 1$ mm, the difference becomes as large as two or three orders of magnitude at $d < 10$ μm. This evidently shows the expectation in Fig. 1; as the probe spacing is reduced, the measurement has a higher surface sensitivity. The results with smaller probe spacings should be more intrinsic to the surface structures because of negligible contribution from the bulk region.

The results are qualitatively described by Ohm's law in classical electromagnetism. If we assume the sample as *a homogeneous and isotropic semi-infinite three-dimensional resistive material*, the resistance R measured by a linear four-point probe method

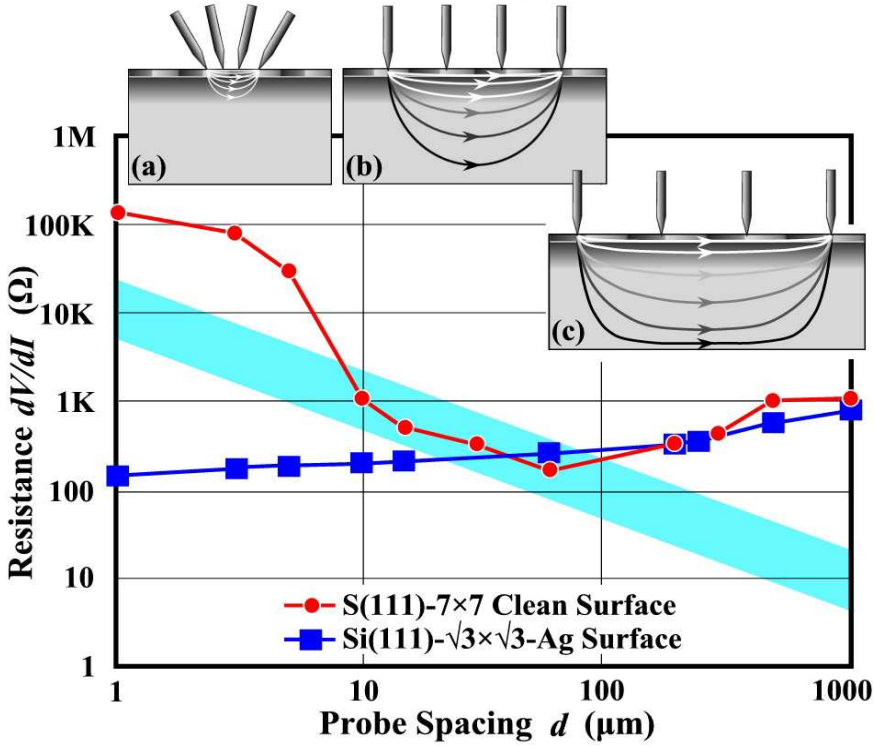

Fig. 6. Probe-spacing dependence of the resistance of a Si crystal, measured at room temperature by the independently driven four-tip STM prober, for the Si(111)-(7×7) clean surface (●) and Si(111)-$(\sqrt{3}\times\sqrt{3})$-Ag surface (■). The insets are schematic illustrations of the current distribution in the sample for the 7×7 surface.

should be

$$R = \rho/2\pi d\,, \tag{1}$$

where ρ is its bulk resistivity (Ω cm). The measured resistance should be inversely proportional to the probe spacing d. This relation is shown in Fig. 6 by a light blue band, because our Si sample has the resistivity of $\rho = 5$–$15\ \Omega$ cm. The experimental data for the 7×7 surface are consistent with this theoretical prediction only at $10\ \mu\text{m} < d < 100\ \mu\text{m}$, while the data points deviate upward from the theory at larger d and smaller d. This feature with comparison to Eq. (1) was confirmed also for silicon crystals of different bulk resistivities. Therefore, we can say that the sample crystal (0.4 mm thick) is regarded as a homogeneous semi-infinite bulk when the probe spacing d is between 10 and 100 μm, because the current distribution does not practically reach the bottom of the crystal, as schematically shown by the inset (b) in Fig. 6. Furthermore, the influence of the surface layer is negligible, since the majority of the measuring current passes through the bulk region because of comparatively large probe spacings.

When d is larger still ($d > 100\ \mu$m), on the other hand, the current penetrates deeper into the crystal and reaches its bottom, as shown in the inset (c) in Fig. 6; the current distribution may be compressed due to the finite thickness of the sample. This effectively raises the measured resistance, corresponding to the data points at $d > 100\ \mu$m, deviating upward from the prediction of Eq. (1). The results at the large d regime are roughly described by a standard form of $R = \rho L/S$, where L is the length of the measured area and S is the cross section of the sample. Since $L = 3d$ and the measuring current spreads laterally on the order of $3d$, $S \sim 3d\cdot t$, where t is the thickness of the sample (0.4 mm). Therefore, $R \sim \rho/t$, and then $R \sim 120$–$400\ \Omega$, which is roughly consistent with the measured data at $d > 100\ \mu$m in Fig. 6.

On the contrary, at the smaller d regime ($d < 10\ \mu$m), which is comparable to the thickness of the surface space-charge layer ($\sim 1\ \mu$m), the current

mainly flows near the surface, as shown in the inset (a); the penetration depth of the current distribution in the sample is similar to the probe spacing in the usual cases. Therefore, the data points in Fig. 6 indicate that the resistance at the surface region is larger than that of the inner bulk, because the data at $d < 10$ μm deviate upward from the light blue band. This conclusion is reasonable when one recalls the fact that the surface space-charge layer beneath the clean 7×7 surface is always a depletion layer, irrespective of the bulk doping concentration and type. This is because the Fermi level at the surface is strongly pinned by the dangling-bond state located at the middle of the band gap.[22,23] Thus the surface region has a higher resistance for the 7×7 surface compared with the inner bulk region.

On the other hand, the d dependence of resistance for the $(\sqrt{3} \times \sqrt{3})$-Ag surface does not fit Eq. (1) at all. According to Ohm's law in classical electromagnetism, when the resistance of *an infinite two-dimensional sheet* is measured by a linear four-point probe of probe spacing d, the measured resistance R is written as

$$R = (\ln 2/2\pi) \cdot R_S \,, \tag{2}$$

where R_S is the sheet resistance (Ω). This means that the measured resistance should be constant, independent of the probe spacing d. The experimental data points for the $(\sqrt{3} \times \sqrt{3})$-Ag surface in Fig. 6 roughly follow this tendency, rather than Eq. (1). As described in detail in the next section, the $(\sqrt{3}\times\sqrt{3})$-Ag surface has a two-dimensional free-electron like surface-state band which is metallic and conductive, and furthermore its surface space-charge layer is always a weak hole-accumulation layer. This is why the surface region has a much higher conductivity than in the bulk.[24] The contribution from the surface-state band dominates the measured conductance, as revealed in the next section. Therefore, the conduction is two-dimensional, rather than three-dimensional.

In this way, by changing the probe spacing from macroscopic distances to microscopic ones, one can switch the conductivity measurement from the bulk-sensitive mode to a surface-sensitive one, so that one can clearly distinguish between 2D conduction and 3D conduction.

2.3. *Surface-state conduction*

The $(\sqrt{3} \times \sqrt{3})$-Ag surface is thus shown to have a much lower resistance, or a much higher surface conductance, than the 7×7 surface. Then, is this due to the surface-space charge layer or surface states? To answer this question, we shall first estimate the conductance through the space-charge layers under the respective surfaces. Since the Fermi-level position in the bulk is known from the impurity doping level (or the bulk resistivity), we have only to know the Fermi-level position at the surface (E_{Fs}). Then we can calculate the band bending beneath the surface and the resulting carrier concentration there, to obtain the conductance through the surface space-charge layer.[25] The brown curve in Fig. 7 shows the space-charge-layer conductance calculated as a function of E_{Fs} for our sample crystal. The conductance on the vertical axis is shown with respect

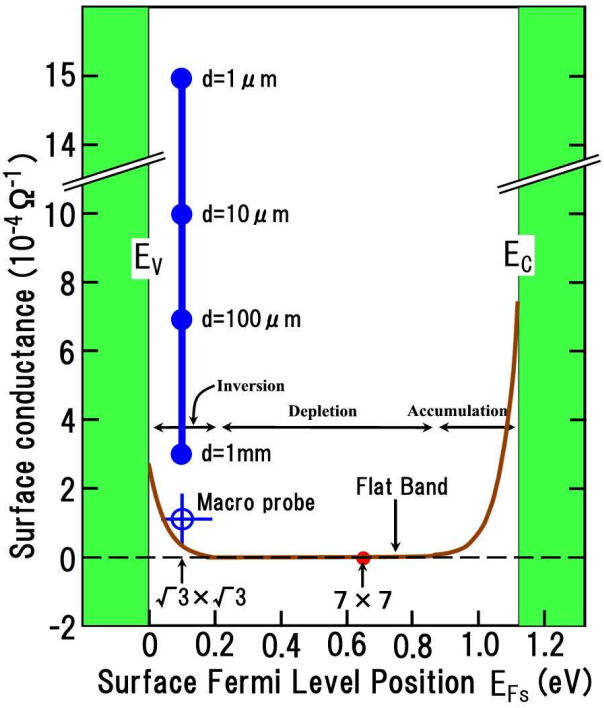

Fig. 7. The brown curve shows conductance through the surface space-charge layer, calculated as a function of the surface Fermi-level position (E_{Fs}). The calculation is done only for E_{Fs} within the band gap. The conductance on the vertical axis is shown with respect to that under the flat-band condition. The experimental data points are plotted at the respective E_{Fs} positions for the $(\sqrt{3} \times \sqrt{3})$-Ag and 7×7 surfaces.

to that under the flat-band condition (where E_{Fs} coincides with E_F in the bulk, 0.75 eV above the bulk valence-band maximum in this case). When E_{Fs} is located around the middle of the bulk band gap, the surface space-charge layer is a depletion layer where the conductance is low. When E_{Fs} is near the bulk conduction-band minimum E_C (valence-band maximum E_V), the layer is an electron (hole) accumulation layer where the conductance is increased due to the excess carriers in the layer.

Fortunately, the E_{Fs} positions at the 7×7 and $(\sqrt{3} \times \sqrt{3})$-Ag surfaces are already known from photoemission spectroscopy measurements[22–24] to be 0.63 eV and 0.1–0.2 eV above E_V, respectively. These do not depend on the bulk doping level, owing to the Fermi-level pinning by metallic surface states. From Fig. 7, then, one can estimate the conductance through the surface space-charge layer below the respective surfaces. Since the 7×7 surface is located in the depletion region and the $(\sqrt{3} \times \sqrt{3})$-Ag is in a weak hole-accumulation region, the latter surface should have a higher conductance than the former by about $5 \times 10^{-5} \Omega^{-1}/\square$.

Since the calculated conductance is not absolute values, but just a change from that under the flat-band condition, we cannot make a straightforward comparison between the calculated conductance and the experimental data. Therefore, we next have to assume that the measured conductance of the 7×7 clean surface is the space-charge-layer conductance only; no surface-state conductance contributes. Then the data point of the 7×7 surface is right on the calculated curve at $E_{Fs} = 0.63$ eV above E_V, as shown in Fig. 7. Since, then, we can obtain the *difference* in conductance between the 7×7 and $(\sqrt{3} \times \sqrt{3})$-surfaces from their measured conductance in Fig. 6, we can plot the results at the E_{Fs} position of the $(\sqrt{3} \times \sqrt{3})$-Ag surface. These are indicated by the bold straight blue line with circles. As shown in Fig. 6, the conductance changes in a wide range, depending on the probe spacing. As the probe spacing is reduced, the measured conductance significantly deviates upward from the calculated curve in Fig. 7. Especially for the probe spacing of 1 μm, the measured conductance is higher than the expected space-charge-layer conductance by more than one order of magnitude. Therefore, the high conductance of the $(\sqrt{3} \times \sqrt{3})$-Ag surface is explained not only by the space-charge-layer conductance, rather, the surface-state conductance dominantly governs the measured value.

If the assumption mentioned above about conductance of the 7×7 surface is not true, i.e. if the surface-state conductance largely contributes to the measured conductance for the 7×7 surface, its data point should be located above the calculated curve in Fig. 7. Then the data points for the $(\sqrt{3} \times \sqrt{3})$-Ag surface also deviate further upward above the calculated curve. This means again that the contribution from the surface-state conductance is larger still. Therefore, the above assumption does not affect the conclusion of the surface-state conductance of the $(\sqrt{3} \times \sqrt{3})$-Ag surface; rather, it makes an underestimate for the surface-state conductance. Since there are reports that the surface-state conductance of the 7×7 surface is 10^{-6}–10^{-8} Ω^{-1},[16,17] the conductance is lower than that of the $(\sqrt{3} \times \sqrt{3})$-Ag surface by 2–4 orders of magnitude, which is negligibly low. In any cases, the conclusion about the $(\sqrt{3} \times \sqrt{3})$-Ag surface is not affected by whether the surface-state conductance contributes on the 7×7 surface.

The surface-state conductance of the $(\sqrt{3} \times \sqrt{3})$-Ag surface was already detected and confirmed with the macroscopic four-point probe method by observing a conductance increase due to carrier doping into the surface-state band.[14] But the microscopic four-point probe method described here has made it possible just by comparing the conductance values between the two surfaces. This is owing to its high sensitivity in measurements of the surface-state electrical conduction.[4] In other words, the microscopic four-point probe, whose probe spacing is comparable to the thickness of the space-charge layer, is an effective tool for detecting and measuring the surface-state conductance of the topmost atomic layers.

In spite of the continuous efforts to detect the surface-state conductance since the 1970's, unambiguous experimental detections have been lacking for a long time.[18] Therefore, the results described above are significant in surface physics, which opens up a new opportunity of study on the transport property of surface electronic states.

For comparison, a data point obtained by a macroscopic four-point probe (probe spacing of about 10 mm) is plotted as an open blue circle in Fig. 7.[21] Since this point is located close to the calculated curve for the surface-space-charge-layer conductance, we cannot say within the experimental

errors that the data point deviates significantly from the calculated curve. Therefore, we could not conclude the contribution of the surface-state conductance just by comparing the measured conductance between the 7×7 and $(\sqrt{3} \times \sqrt{3})$-Ag surfaces in the case of the macro-four-point probe method.[21] This is because the macro-probe method does not enable precise measurements of surface-state conductance for lack of sufficient surface sensitivity; the bulk conductance mainly contributes to the measured values.

In spite of these analyses, however, some readers may think that this reasoning is not convincing. Since, according to Fig. 7, the $(\sqrt{3} \times \sqrt{3})$-Ag surface has an extremely high surface-state conductance compared with the conductance through the surface space-charge layer, one may claim that the surface-state conductance should be detected even by the macroscopic four-point probe method in spite of its low surface sensitivity. And its measured value should be the same as those obtained by the micro-four-point probe method once the contribution from the bulk conductance is subtracted. Why does the measured surface conductance depend on the probe spacing?

As described by Eq. (2), if the sample is regarded as an infinite 2D and homogeneous resistive sheet, the measured resistance should be constant, independent of the probe spacing d. This is because the carrier scattering centers are distributed densely and homogeneously; in other words, the spacing among the scattering centers is much smaller than the probe spacing, so that R_S should be regarded as constant irrespective of the size of the measured area, or the probe spacing d. The data points in Figs. 6 and 7 evidently contradict this prediction.

This may be because the carrier scattering at surface defects is *effectively* different between in the macroscopic measurement and in the microscopic one. Let us take atomic steps on a surface as an example; as shown in the next section, atomic steps scatter carriers, and cause resistance, resulting in serious influence on the conductance. Even if the average step–step separation is the same, the influence of the step on resistance may depend on the degree of wandering of steps in macroscopic measurements; imagine that meandering steps may scatter the carriers more frequently than arrays of straight steps. But when the conductance is measured in microscopic regions where the probe spacing is comparable to the distance between adjacent steps (i.e. terrace width), the steps should be regarded as straight in the measured area even if the steps are winding in the macroscopic scale. Therefore the *effective* carrier scattering may be reduced. Thus the resulting sheet resistance R_S can change depending on the scale of the measured areas. The conductance measured in microscopic regions should be an intrinsic value, due to reduction of the influence of atomic steps and other surface defects.

Next, let us estimate the mean free path L of the surface-state carriers. Since, as mentioned in the previous subsection, the surface state of $(\sqrt{3} \times \sqrt{3})$-Ag has a nearly free-electron-like band in two dimensions, the sheet conductance σ_{SS} $(= 1/R_S)$ is written by the Boltzmann picture as

$$\sigma_{SS} = S_F \cdot e^2 L / 2\pi h \,, \tag{3}$$

where S_F is the circumference of the Fermi disk ($S_F = 2_\pi k_F$, where k_F is the Fermi wave number), h is Planck's constant and e is the elementary charge. Since k_F is already measured by angle-resolved photoemission spectroscopy,[14,26] $k_F = 0.15 \pm 0.02$ Å^{-1}, S_F can be calculated. On the other hand, from the data at $d = 1$ μm in Fig. 7, the surface-state conductance is $\sigma_{SS} = 1.5 \times 10^{-3}$ $\Omega^{-1}/\square$. Then, by substituting these values into Eq. (3), we obtain $L = 25 \pm 3$ nm for our sample at room temperature (RT). This value is smaller than typical step–step interval and domain size (~ 100 nm) by nearly an order of magnitude, meaning that the surface-state carriers are scattered dominantly by phonons and surface defects other than atomic steps and domain boundaries. This means a diffusive conduction even within single domains and terraces at RT. But, for the details of the carrier scattering mechanism, we have to measure the temperature dependence of conductance in a wide temperature range, which we are now preparing to do. The important point here is that even when the surface-state carriers are scattered by some irregularities, *they are not necessarily scattered into the bulk-state bands.* The surface-state carriers can continue to run through the surface states for a distance much longer than the mean free path, so that the probes of several-μm spacing can effectively detect the surface-state conductance. The scattering rate of the surface-state carriers into the bulk states depends on the relation between the bulk and surface band structures. Because the surface-state

band contributing to the electrical conduction is located within the energy gap in the bulk-state bands for the $(\sqrt{3} \times \sqrt{3})$-Ag case — in other words, because the surface state is energetically isolated from the bulk states — the surface-state carrier should have a longer lifetime.

Next, let us estimate the mobility μ of the surface-state carriers. The mean free path L can be written as $L = \tau V_F$, where τ is the relaxation time and V_F is Fermi velocity. The mobility μ is written as

$$\mu = e\tau/m^* , \tag{4}$$

where m^* is the effective mass of surface-state carriers. Since we know m^* and k_F from the band dispersion measured by angle-resolved photoemission spectroscopy,[14,26] $m^* = (0.29 \pm 0.05)m_e$, where m_e is free electron mass, we can calculate $V_F = hk_F/m^*$. Then we can obtain τ, too. As a result, we obtain $\mu = 250 \pm 50\ \mathrm{cm}^2/V \cdot s$. This value is lower than that of conduction electrons in three-dimensional bands of a Si bulk crystal, 1500 $\mathrm{cm}^2/V \cdot s$, by nearly an order of magnitude. This means that the surface-state carriers are scattered by phonons and defects more seriously than the carriers in bulk. It should also be noted that the mobility obtained here is higher than that previously obtained by the macro-four-point probe method by an order of magnitude.[14] This means, as mentioned above, that the influence of carrier scattering by surface defects is effectively reduced in microscopic measurements compared with macroscopic measurements, resulting in a larger mobility. If one can measure the conductivity of almost defect-free regions with further smaller probes, the measured mobility will apparently be further increased.

In the next section, we shall introduce another type of microscopic four-point probe method and their preliminary results that directly show the influence of atomic steps on the conductance.

3. Monolithic Micro-Four-Point Probes

3.1. *Device and apparatus*

Figure 8(a) shows a scanning electron micrograph (SEM) of a chip for a micro-four-point probe, which is produced by using silicon microfabrication technology at the Microelectronics Center of Denmark Technical University.[4] The technique is similar to that for producing cantilevers of atomic force microscopy. The probes are now commercially available.[27] One can choose the probe spacing ranging from 2 μm to 100 μm, while probes of several-hundred-nm spacing are under development. The substrate is an oxide-covered silicon crystal, on which a metal layer is deposited to make conducting paths. The metal layer covers the very end of four cantilevers so that they can make direct contact with the sample surface. The angle between the cantilever and the sample surface is about 30°, as shown by the inset in Fig. 8(a), so that the cantilevers bend to make contact with the sample easily for all of the four cantilevers even if the tips of the four cantilevers are not strictly aligned parallel to the sample surface.

The probe is installed in a UHV-SEM-RHEED chamber, as schematically shown in Fig. 9.[3] Owing to a field-emission electron gun in the SEM column, this machine enables *in-situ* characterization of the surface structures of the sample by SEM, microbeam-RHEED and SREM observations, as well as monitoring of the probe position. The sample surface can be cleaned by direct current heating, and materials can be *in-situ* deposited from evaporators to prepare adsorbate-induced surface superstructures and epitaxial atomic layers on the specimen surface. These abilities are the same as for the four-tip STM prober system described in the previous section. Because of the glancing incidence of the electron beam to enhance the surface sensitivity in imaging, SEM images shown here are vertically shortened by about a factor of 3 compared with the horizontal direction in images.

The micro-four-point-probe chip is moved away from the sample by using linear motion feedthrough during sample preparation. Then the chip is made to approach the sample with the coarse-motion feedthrough, and its final fine positioning is done by three-axis piezo-actuators (MicroSlide, Omicron) with a precision of about 20 nm, resulting in gentle contact with the aimed area on the sample under SEM observation.

Figures 8(b)–8(c) are SEM images of a sample [Si(111)-(7 × 7) clean surface] and the micro-four-point probe (8 μm spacing) making contact with the sample. The probes look to make contact with the sample surface vertically in these images due to the shortening in the vertical direction by the glancing

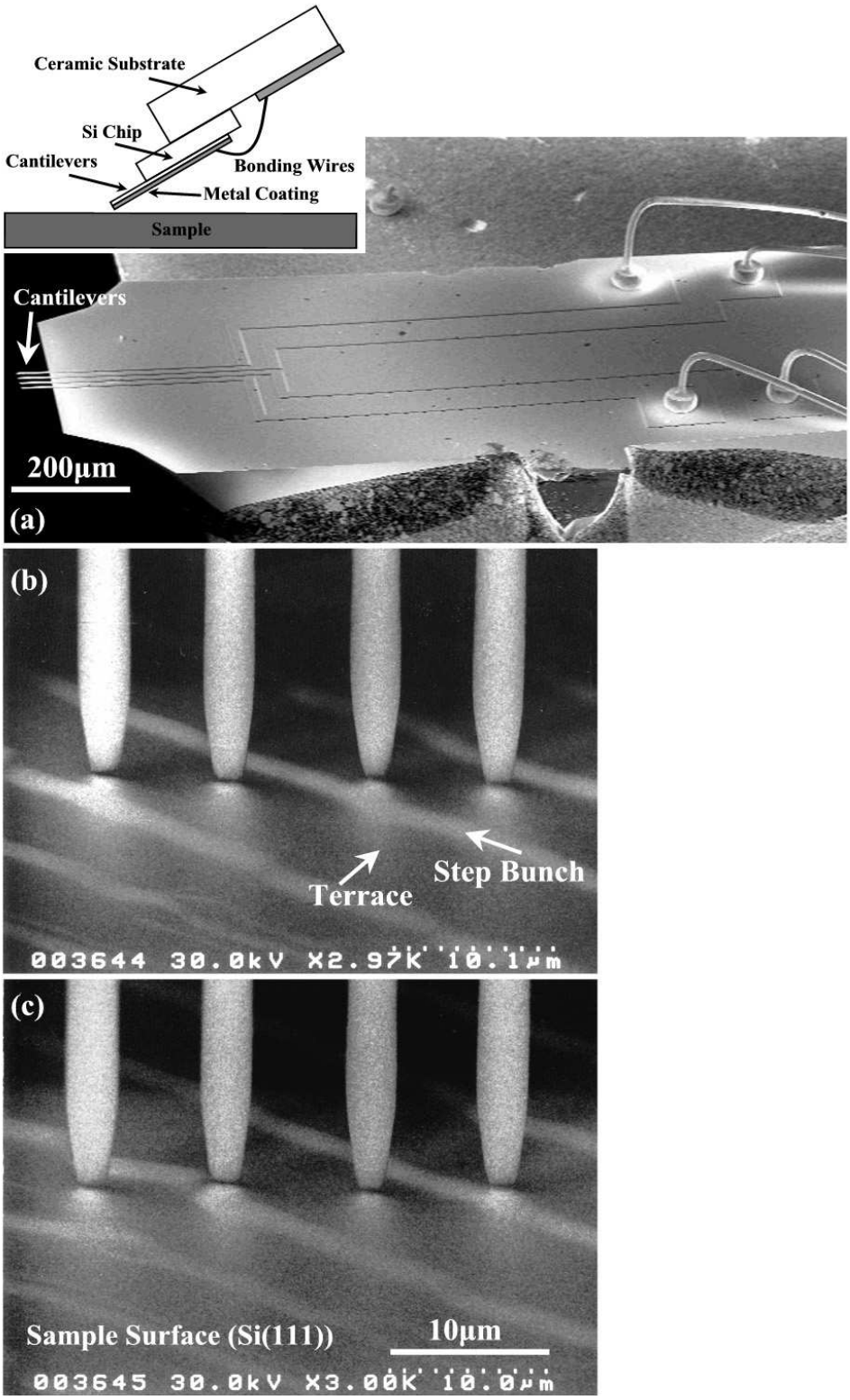

Fig. 8. Micro-four-point probe. (a) SEM image of the chip. The inset shows a schematic side view of the probe making contact with a sample surface. (b), (c) Glancing-incidence SEM images of a micro-four-point probe (probe spacing 8 μm), making contact with a sample [Si(111)-(7 $\times$ 7) clean surface] in UHV during the measurement of conductance. The probe is shifted laterally from (b) to (c) by about 5 μm using piezoactuators for fine positioning.

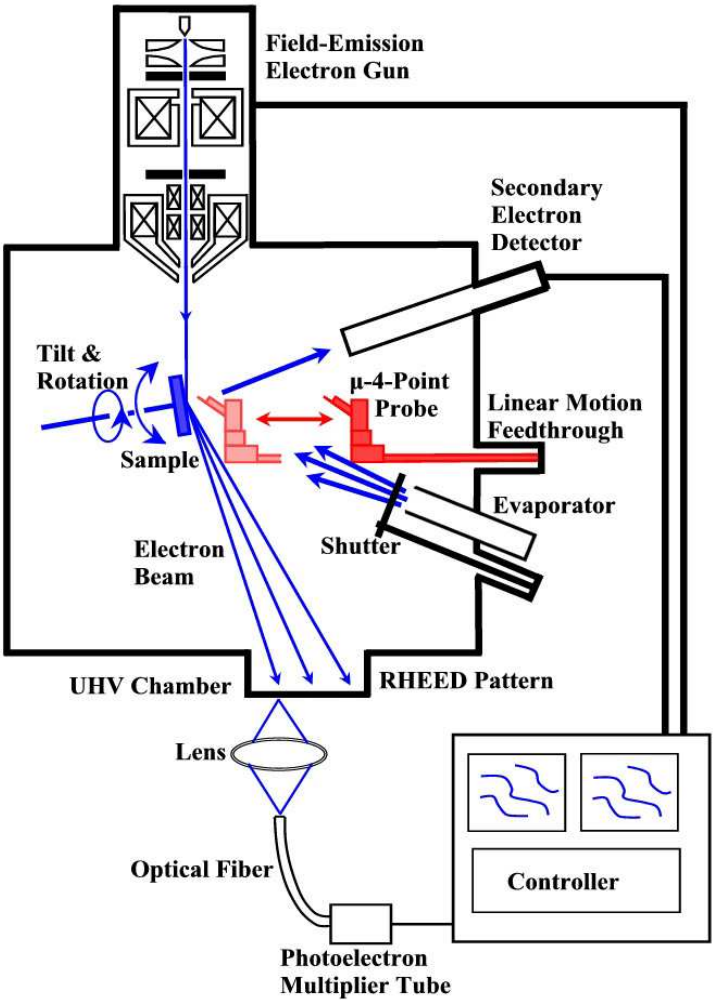

Fig. 9. Schematic of a UHV-SEM-RHEED system, combined with the micro-four-point probe system.

incidence of the electron beam; the probes actually contact in a way described in the inset of Fig. 8(a). The probe is shifted laterally by about 5 μm in Fig. 8(c) from the position in Fig. 8(b). Thus, the local conductance of the aimed areas can be measured by fine positioning of the probe with the aid of *in-situ* SEM. Compared with the four-tip STM prober described in the previous section, it is much easier to bring the probes into contact with the sample, though we cannot change the probe spacing. These two methods are complementary to each other in this sense.

3.2. *Influence of atomic steps*

On the usual (nominally) flat (111) surface of a Si crystal, atomic steps distribute regularly with a step–step distance of 0.1–1 μm (regular-step surfaces) due to slight misorientation in cutting the crystal. Therefore, to measure the step influence by micro-four-point probes of several-μm probe spacing (Fig. 8), step-free regions (terraces) should be made wider than the probe spacing by using the phenomenon of step bunching. Then the probes enable the conductance measurements at terrace areas of almost step-free or step-bunch areas with hundreds of steps accumulated, so that the influence of atomic steps on conductance can be extracted by comparing the data between such regions.

Fortunately, a method to control the step configuration for obtaining wide terraces has already been developed.[28] As shown in Fig. 10(a), arrays of small holes are made on a nominally flat (but actually vicinal) Si(111) crystal surface using

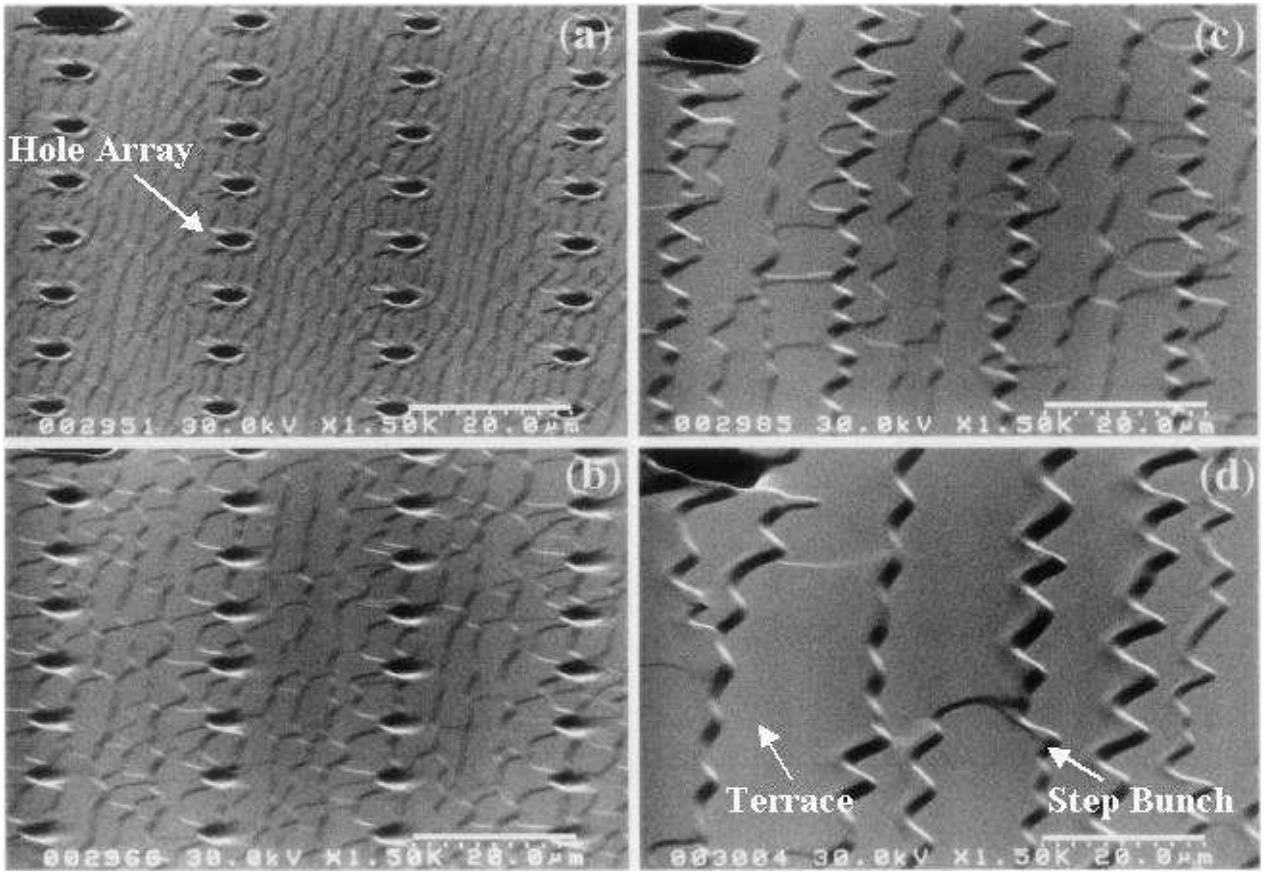

Fig. 10. Series of *in-situ* glancing-incidence UHV-SEM images, showing a process of step bunching on a Si(111) surface with small-hole array patterning. By repeated flash-heating up to 1250°C, the surface turns clean to become the 7×7 structure, and simultaneously atomic steps move back and are pinned at positions of the initial hole arrays.

suitable etching techniques before inserting the sample into UHV. The diameter and depth of the holes are around 1 μm, and their separation is around 20 μm in this case. When one repeats flash heating of the Si crystal up to 1250°C in UHV by direct current flowing through the crystal in a direction perpendicular to the hole arrays, the sample surface is cleaned. Simultaneously the atomic steps move and the holes disappear, as shown in Figs. 10(b)–10(c). This is due to sublimation of Si atoms from the surface, resulting in moving back of atomic steps. With enough cycles of flash heating, finally as shown in Fig. 10(d), atomic steps are accumulated at the positions of initial hole arrays, i.e. step bunches, between which wide and flat terraces that are almost step-free are created. The width of the terraces can be controlled by the initial hole-array separation; in Fig. 10, it is 20 μm, which is wider than the probe spacing. A step-bunch region contains monatomic steps of around 300, separated by very narrow terraces, much like step fields on a mountain slope. The narrow terraces in the step-bunch regions are the usual (111) surfaces, so that the regions are not faceted in this case.

The sample surface in Figs. 8(b)–8(c) was prepared with this method; brighter bands about 2 μm wide running parallel to each other on the sample surface are step bunches, while darker areas about 10 μm wide between the step bunches are flat terraces. In Fig. 8(b), a step bunch runs between the inner pair of probes, so that a voltage drop is measured across the step bunch, while in Fig. 8(c) the probes were shifted laterally to put the inner pair of probes on a single terrace with no step-bunch crossing. By comparing the measured resistances at these two positions, the result should contain more influence of

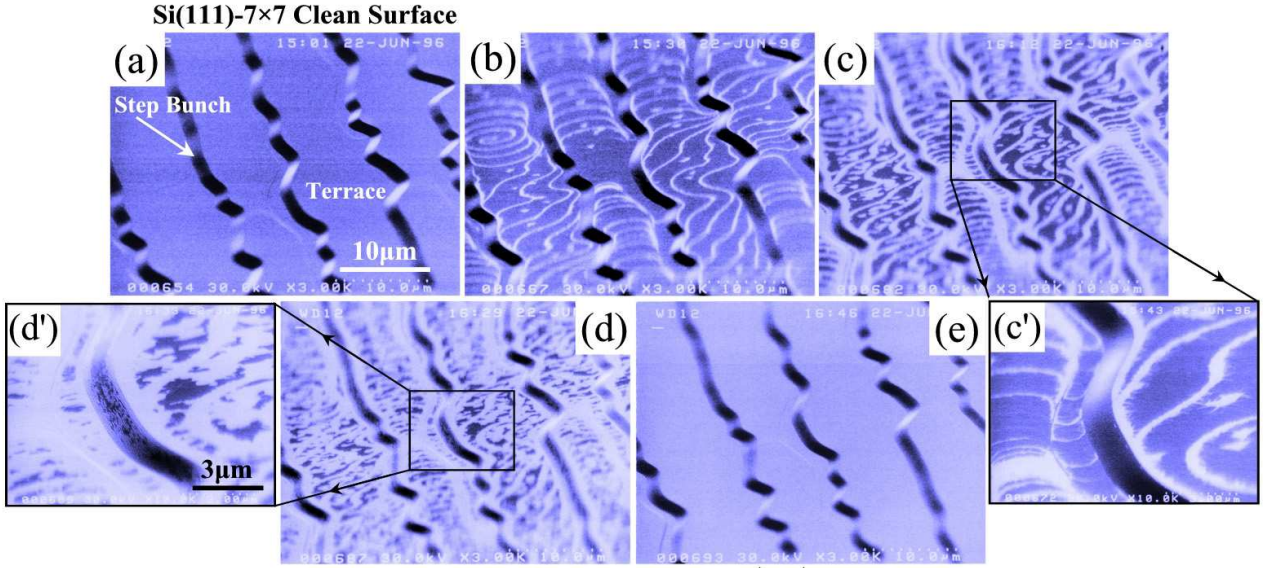

Fig. 11. Series of *in-situ* glancing-incidence UHV-SEM images during Ag deposition on a step-bunched Si(111)-(7×7) clean surface kept at 450°C. With increasing Ag coverage, the brighter thin domains [$(\sqrt{3}\times\sqrt{3})$-Ag structure] appear at monatomic step edges and expand, while the darker domains (7×7 clean structure) shrink [(b)–(d)]. Finally, the surface is wholly covered by the brighter domains homogeneously in (e). (c′) and (d′) are magnified images, showing that narrow terraces within step-bunch regions also change the structure. So the step bunches can be simply regarded as arrays of hundreds of monatomic steps. By comparing (a) with (e), it is noticed that the whole morphology of the surface does not change during the structure conversion from 7×7 to $(\sqrt{3}\times\sqrt{3})$-Ag.

steps in (b) than in (c). In this way, the micro-four-point probe enables the conductance measurements of selected microscopic areas by precise positioning.

Figure 11 shows *in-situ* observations of SEM during Ag deposition on such a step-bunched Si(111)-(7×7) clean surface [Fig. 11(a)] kept at 450°C.[20] Bright thin lines begin to appear at the initial stage of deposition, as shown in Fig. 11(b). The deposited Ag atoms migrate on the surface at 450°C, and are then captured by atomic steps, where the 7×7 structure converts into the $(\sqrt{3}\times\sqrt{3})$-Ag structure. The bright thin areas are the domains of the $(\sqrt{3}\times\sqrt{3})$-Ag structure thus formed along steps, while darker areas are domains of the clean 7×7 structure. This image shows that the terrace areas about 10 μm wide are not completely step-free; rather, several monatomic steps run across the wide terraces. But this is a much lower step density compared with the step-bunch areas where more than 100 steps are accumulated.

With increase of Ag coverage, the brighter areas spread as seen in Figs. 11(c) and 11(c′), and simultaneously the $(\sqrt{3}\times\sqrt{3})$-Ag domains appear on terraces as well as near step edges, as in Figs. 11(d) and 11(d′). Finally, with deposition of 1 ML of Ag, the terraces and step bunches are wholly covered by the brighter domains, as shown in Fig. 11(e). By comparing Fig. 11(a) with Fig. 11(e), the surface morphology of terrace–step-bunch structure is not changed by the structure conversion from the 7×7 to $(\sqrt{3}\times\sqrt{3})$-Ag. The narrow terraces in the step-bunch area have the same 7×7 and $(\sqrt{3}\times\sqrt{3})$-Ag structures as on the wide terraces in (a) and (e), respectively.

Figures 12(a) and 12(b) show "line profiles" of resistance measured with the micro-four-point probe (probe spacing $d = 8$ μm) by shifting it along a line across step bunches on such step-bunched Si(111)-(7×7) clean and $(\sqrt{3}\times\sqrt{3})$-Ag surfaces at RT, respectively. The horizontal axis shows the position of the probe on the line; the data points are plotted at the position of the center of the micro-four-point probe. The surface morphology observed by SEM is schematically shown at the bottom of each graph; the vertical scale is exaggerated. These results show that the resistance changes drastically from place to place. As expected, when the inner pair of probe cross over a step bunch as shown in Fig. 8(b) (such

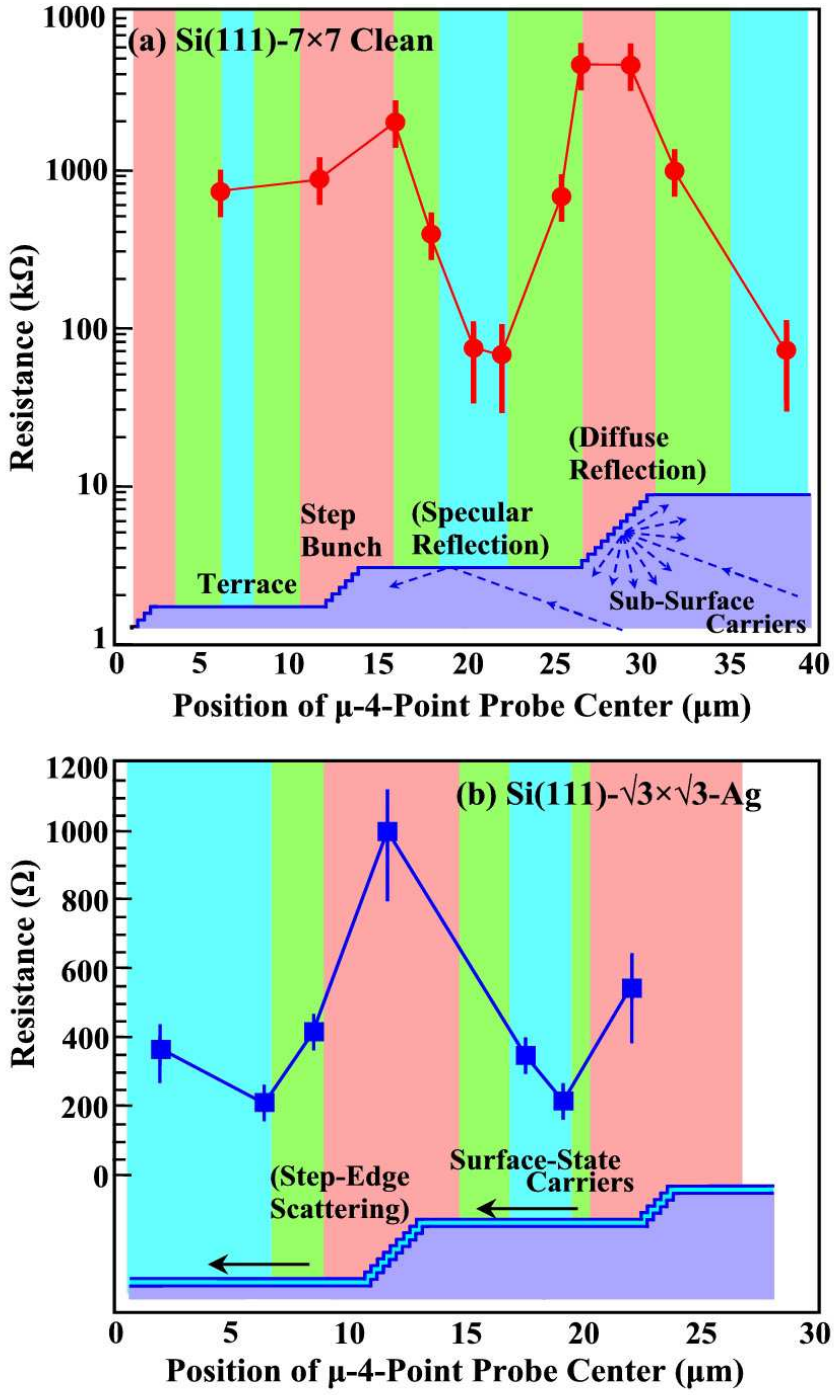

Fig. 12. "Line profile" of resistance of (a) Si(111)-(7 × 7) clean and (b) Si(111)-($\sqrt{3} \times \sqrt{3}$)-Ag surfaces, obtained by shifting the micro-four-point probes (8 μm probe spacing) along a line across step bunches on the surfaces. The surface morphology of the sample surface, which was determined by SEM, is schematically drawn at the bottom of each graph. The data points are plotted at the positions of the center of the four-point probes. Red areas show a situation where the voltage drop is measured by the inner pair of probes across a step bunch [like in Fig. 8(b)]. Blue areas show a situation where the two inner probes make contact on a single terrace [like in Fig. 8(c)]; no step bunch runs between the inner probes. Green areas show a situation where one of the inner probes is on a terrace and the other probe is on a step-bunch region.

a situation occurs at red areas in Fig. 12), the measured resistance is higher. When the inner pair of probes make contact on the same terrace as shown in Fig. 8(c) without crossing a step bunch (such a situation occurs at blue areas in Fig. 12), lower resistance values are obtained. The 7×7 and $(\sqrt{3} \times \sqrt{3})$-Ag surfaces show qualitatively the same results, but they are quite different in magnitude of change.

An important issue should be commented on here. In general, the four-point probe method works only for homogeneous samples both in the surface-parallel direction and in the depth direction. But the present sample is not the case; the resistance at the step-bunch areas is higher than that on the terraces. So the measured resistances in Fig. 12 are not the true values of the respective areas. We need a kind of "deconvolution" from the measured data to obtain the true values. Such a calculation will be published elsewhere.[29] But we can do qualitative discussions from the raw data.

Since for the $(\sqrt{3} \times \sqrt{3})$-Ag surface, as described in the previous section, the conductance is dominated by the surface state, the result in Fig. 12(b) means that the surface-state conduction is actually interrupted at step edges. This is very reasonable when one recalls STM pictures of so-called electron standing waves near step edges on this surface directly observed by low-temperature STM,[30] which is nothing but the direct view of carrier scattering at steps. Figure 12 shows the first direct measurement of resistance caused by such step-edge scattering, from which we will be able to deduce the resistance due to a single monatomic step and transmission (and reflection) coefficient of the electron wave function of electrons there.

At this moment, we cannot directly detect the influence of a single atomic step on the conductance. It is still unclear whether the influence of a step bunch can be regarded as a simple multiple of the influence of a single atomic step. It may depend on whether the transport is diffusive or ballistic at the step-bunch regions. Strain fields, furthermore, are created in the step-bunch regions due to the narrow step–step distance, which may cause additional influence on the conductivity.

As shown in the previous section, the conductance of the 7×7 surface is lower than that of the $(\sqrt{3} \times \sqrt{3})$-Ag surface by more than two orders of magnitude, which is reasonable when one recalls the reports about the surface-state conductance of the 7×7 surface,[16,17] giving it as small as 10^{-6}–$10^{-8}\ \Omega^{-1}$. The surface-state electrical conduction, if any, is interrupted by steps in the same way as on the $(\sqrt{3}\times\sqrt{3})$-Ag surface. The surface-space-charge-layer conductance, which is also low because of the depletion condition beneath the (7×7)-reconstructed layer, is also influenced by the step bunches. The carriers flowing through the surface space-charge layer should be perturbed by the step bunches on the surface. This is because, according to the classical view of Fuchs–Sondheimer about carrier scattering at surfaces.[31,32] the carriers are scattered diffusively at the step bunch areas because of the surface roughness, as illustrated at the bottom of Fig. 12(a), while the carriers are reflected specularly at flat terraces. The diffusive scattering causes additional resistance, while the specular reflection does not. Alternatively, excess charges accumulated in electronic states characteristic of the step edges may locally disturb the band bending just below the step-bunch regions, resulting in carrier scattering in the surface space-charge layer. In this way, a higher resistance is most likely to be detected across the step bunches not only for the surface-state carriers but also for the carriers flowing through the surface space-charge layer.

Although the surface states are interrupted at step edges, the surface-state carriers can pass through the step edges with some probability, penetrating into the surface states on the adjacent terraces. The transmission probability at the step edges is less than 100%, but not zero. If the surface-state electrons have extended wave functions like for the $(\sqrt{3} \times \sqrt{3})$-Ag structure, the transmission probability may be higher because of a larger overlap of wave functions with that on the neighboring terraces. On the contrary, the transmission probability may be lower for surface states having a localized nature like that of the 7×7 surface, because of the negligible overlap of the wave function with that of the adjacent terraces. So the influence of steps on the surface-state conductance may be more significant for the latter case. Actually, the resistance increases by two orders of magnitude at step bunch regions for the 7×7 surface [Fig. 12(a)], while it increases by only a factor of 4 for the $(\sqrt{3} \times \sqrt{3})$-Ag surface [Fig. 12(b)]. Such an intuitive expectation should be confirmed by theoretical estimates.

4. Concluding Remarks

The microscopic four-point probe methods described here are unique and powerful tools in surface science, especially for studying surface transport, and are expected to be increasingly important, because the electrical conduction through one or two atomic layers on surfaces may play essential roles in nanometer-scale science and technology. The reader may see the usefulness from the preliminary results described here. Of course, the probes can be applied not only for the study of surface transport, but also for transport properties of microscopic and nanometer-scale objects. The probes will be used under various conditions, such as at low and high temperatures, under magnetic field, and under illuminations. We have already constructed a system for the micro-four-point probe measurements at temperatures down to 10 K in UHV. The results will be reported elsewhere.

An important issue to be discussed about the four-point probe method is the contact points between the probe and the sample surface. Although, as mentioned in Sec. 1, the contact resistance is virtually eliminated in the four-point probe measurements, the contact conditions may influence the measurement results, especially for the microscopic probes. Since the contacts are direct ones, the atomic arrangements at the very points of contact may be destroyed. Then, the electronic structures, including band bending, can change very close to the probe contacts. Such distorted regions spread on the order of Debye lengths. Therefore, when the probe spacing is comparable to the Debye lengths, we will have to take into account this effect. To avoid this type of disturbance, the probe contacts should be tunnel contacts, especially for nanometer-scale four-point probes.

Acknowledgments

This work was done under a Grant-in-Aid from the Ministry of Education, Science, Culture, and Sports of Japan, including the International Collaboration Program. The four-tip STM prober was constructed during the Core Research for Evolutional Science and Technology of the Japan Science and Technology Corporation.

References

1. For a review, see: S. Hasegawa, X. Tong, S. Takeda, N. Sato and T. Nagao, *Prog. Surf. Sci.* **60**, 89 (1999).
2. S. Hasegawa, *J. Phys.: Cond. Matter* **12**, R463 (2000).
3. I. Shiraki *et al.*, *Surf. Rev. Lett.* **7**, 533 (2000).
4. C. L. Petersen *et al.*, *Appl. Phys. Lett.* **77**, 3782 (2000).
5. I. Shiraki *et al.*, *Surf. Sci.* **493**, 643 (2001).
6. S. Hasegawa, I. Shiraki, F. Tanabe and R. Hobara, *Current Appl. Phys.* **2**, 465 (2002).
7. S. Hasegawa, I. Shiraki, T. Tanikawa, C. L. Petersen, T. M. Hansen, P. Boggild and F. Grey, *J. Phys.: Cond. Matter* **14**, 8379 (2002).
8. O. Pfennigstorf, A. Petkova, H. L. Guenter and M. Henzler, *Phys. Rev.* **B65**, 045412 (2002).
9. M. Henzler, T. Luer and J. Heitmann, *Phys. Rev.* **B59**, 2383 (1999).
10. M. Jalochowski, M. Hoffman and E. Bauer, *Phys. Rev. Lett.* **76**, 4227 (1996).
11. M. Jalochowski, *Prog. Surf. Sci.* **48**, 287 (1995).
12. K. R. Kimberlin and M. C. Tringides, *J. Vac. Sci. Technol.* **A13**, 462 (1995).
13. L. Gavioli, K. R. Kimberlin, M. C. Tringides, J. F. Wendelken and Z. Zhang, *Phys. Rev. Lett.* **82**, 129 (1999).
14. Y. Nakajima *et al.*, *Phys. Rev.* **B56**, 6782 (1997); *Phys. Rev.* **B54**, 14134 (1996).
15. K. Yoo and H. H. Weitering, *Phys. Rev.* **B65**, 115424 (2002); *Phys. Rev. Lett.* **87**, 026802 (2001).
16. S. Heike *et al.*, *Phys. Rev. Lett.* **81**, 890 (1998).
17. Y. Hasegawa *et al.*, *Surf. Sci.* **358**, 32 (1996).
18. M. Henzler, in *Surface Physics of Materials I*, ed. J. M. Blakely (Academic, New York, 1975), p. 241.
19. P. Boggild *et al.*, *Rev. Sci. Instrum.* **71**, 2781 (2000), *Adv. Mater.* **12**, 947 (2000).
20. For a review, see: S. Hasegawa *et al.*, *Jpn. J. Appl. Phys.* **39**, 3815 (2000).
21. C.-S. Jiang, S. Hasegawa and S. Ino, *Phys. Rev.* **B54**, 10389 (1996).
22. F. J. Himpsel, G. Hollinger and R. A. Pollak, *Phys. Rev.* **B28**, 7014 (1983).
23. J. Viernow *et al.*, *Phys. Rev.* **B57**, 2321 (1998).
24. S. Hasegawa *et al.*, *Surf. Sci.* **386**, 322 (1997).
25. For fundamentals of semiconductor surfaces, see e.g: W. Moench, *Semiconductor Surfaces and Interfaces* (Springer, Berlin, 1995).
26. X. Tong *et al.*, *Phys. Rev.* **B57**, 9015 (1998).
27. Visit http://www.capres.com
28. T. Ogino, *Surf. Sci.* **386**, 137 (1997).
29. T. M. Hansen *et al.*, *J. Appl. Phys.*, submitted.
30. N. Sato *et al.*, *Phys. Rev.* **B59**, 2035 (1999).
31. E. H. Sondheimer, *Adv. Phys.* **1**, 1 (1952).
32. K. Fuchs, *Proc. Cambridge Philos. Soc.* **34**, 100 (1938).